## SOLIDS AND LIQUIDS

# Surface Enhanced Raman Scattering of Light by ZnO Nanostructures

**A. G. Milekhin[a,b,*], N. A. Yeryukov[a], L. L. Sveshnikova[a], T. A. Duda[a], E. I. Zenkevich[c],
S. S. Kosolobov[a], A. V. Latyshev[a,b], C. Himcinski[d], N. V. Surovtsev[e], S. V. Adichtchev[e],
Zhe Chuan Feng[f], Chia Cheng Wu[g], Dong Sing Wuu[g], and D. R. T. Zahn[h]**

[a] *Rzhanov Institute of Semiconductor Physics, Siberian Branch of the Russian Academy of Sciences,
pr. Akademika Lavrentieva 13, Novosibirsk, 630090 Russia*
\* e-mail: milekhin@thermo.isp.nsc.ru
[b] *Novosibirsk State University, ul. Pirogova 2, Novosibirsk, 630090 Russia*
[c] *Belarussian National Technical University, pr. Nezavisimosti 65, Minsk, 220072 Belarus*
[d] *Institut für Theoretische Physik, Technische Universität Bergakademie Freiberg, Gellert-Bau,
Leipziger Str. 23, Freiberg, 09596 Germany*
[e] *Institute of Automation and Electrometry, Siberian Branch of the Russian Academy of Sciences,
pr. Akademika Koptyuga 1, Novosibirsk, 630090 Russia*
[f] *Graduate Institute of Photonics and Optoelectronics, National Taiwan University,
1 Roosevelt Rd. Sec. 4, Taipei, 106 Taiwan, R.O.C.*
[g] *Department of Materials Science and Engineering, National Chung Hsing University,
250 Kuo Kuang Road, Taichung 40227 Taiwan R.O.C.*
[h] *Institute of Physics, Semiconductor Physics, Chemnitz University of Technology, Reichenhainer Str. 70,
Neues Physikgebäude (NPhG), Raum P150, Chemnitz, 09107 Germany*
Received March 14, 2011

**Abstract**—Raman scattering (including nonresonant, resonant, and surface enhanced scattering) of light by optical and surface phonons of ZnO nanocrystals and nanorods has been investigated. It has been found that the nonresonant and resonant Raman scattering spectra of the nanostructures exhibit typical vibrational modes, $E_2$(high) and $A_1$(LO), respectively, which are allowed by the selection rules. The deposition of silver nanoclusters on the surface of nanostructures leads either to an abrupt increase in the intensity (by a factor of $10^3$) of Raman scattering of light by surface optical phonons or to the appearance of new surface modes, which indicates the observation of the phenomenon of surface enhanced Raman light scattering. It has been demonstrated that the frequencies of surface optical phonon modes of the studied nanostructures are in good agreement with the theoretical values obtained from calculations performed within the effective dielectric function model.

**DOI:** 10.1134/S1063776111140184

## 1. INTRODUCTION

It is known that the phenomenon of surface enhanced Raman scattering of light consists in abruptly (up to $10^6$ times) increasing intensity of light scattering by molecules located either directly on the surfaces of metals or metal clusters or in the vicinity of these surfaces. Owing to the surface enhanced Raman scattering, significant advances have been achieved in research of optical and vibrational properties of organic and biological materials [1]. Surface enhanced Raman scattering has been successfully used for detecting and analyzing small amounts of organic substances ($5 \times 10^{-7}$ mol) [2, 3] down to molecular dimensions, including single molecules [4, 5]. Furthermore, considerable progress has been made in understanding the mechanisms responsible for surface enhanced Raman scattering [6]. Recent investigations have demonstrated that the surface enhanced Raman scattering has also been observed in inorganic materials, in particular, in GaN semiconductor nanorods [7], CdS quantum dots [8], carbon nanotubes [9], etc.

Interest expressed by researchers in the ZnO compound is associated with the fact that this direct-band-gap semiconductor with a relatively large band gap (3.37 eV) exhibits an intense photoluminescence in the ultraviolet spectral range and can be considered as a promising material for the use in the design of the elemental base of nano- and optoelectronics, in particular, sources and detectors of ultraviolet radiation [10]. A decrease in the dimensions of semiconductor materials, including ZnO, down to the nanometer scale leads to a significant modification of their optical and vibrational properties. In this case, the surface effects play an increased role due to the large ratio of

the number of atoms on the surface to the number of atoms in the bulk of the nanostructures.

Raman scattering spectroscopy has been widely used for studying vibrational spectra of ZnO-based nanostructures, such as nanowires [11−13] and quantum dots [14−20], with different shapes and sizes. In particular, nonresonant and resonant Raman scattering in ZnO nanostructures has been investigated [15, 16], the influence of the dimension of nanostructures on the spectrum of their optical phonons has been elucidated [17, 18], and the dependence of the frequencies of surface optical phonons on the permittivity of the matrix has been determined [19, 20]. Also reported has been the observation of the enhancement of Raman scattering in ZnO/metal nanocomposites. In particular, under resonance conditions (when the laser excitation energy is close to the energy of interband transitions in ZnO nanostructures, but in the absence of resonance with the energy of the localized plasmon in metallic clusters), the enhancement of the Raman scattering by the $A_1$ longitudinal optical (LO) mode has been observed in the presence of Ag clusters both for the ZnO crystalline films [21] and ZnO needle nanostructures [22] and for the nanocomposites consisting of ZnO quantum dots and Au clusters [23, 24].

This paper reports on the observation of surface enhanced Raman scattering of light by surface optical phonons for two types of ZnO-based nanostructures, such as nanorods (or nanocolumns) and free-standing nanocrystals, which made it possible to perform a comparative analysis of the phonon spectra of nanostructures for one material with different surface morphologies. It is important to note that, in this work, during the process of surface enhanced Raman scattering, the excitation energy coincides with the energy of the localized plasmon in metallic clusters, but differs from the energy of interband transitions in nanostructures.

## 2. SAMPLE PREPARATION AND EXPERIMENTAL TECHNIQUE

The studied structures with ZnO nanorods were produced through the gas-phase epitaxy from organometallic compounds on substrates prepared from the sapphire oriented in the (0001) direction. A detailed description of the formation of nanorods is presented in [25].

Zinc oxide nanocrystals were formed using the Langmuir−Blodgett technology. For this purpose, zinc behenate films with a thickness of 270 monolayers (ML) were applied on the Si(001) substrates coated with a 100-nm-thick platinum layer. The formation of ZnO nanocrystals was performed through thermal oxidation of zinc behenate films in air at a temperature of 400°C. Thermal oxidation resulted in the removal of the organic matrix and in the formation free-standing ZnO nanocrystals.

Silver nanoclusters on the surfaces of both types of structures were prepared by means of the evaporation in ultra-high vacuum.

The energies of interband electronic transitions in nanocrystals and the energies of localized surface plasmons in silver clusters were determined from the positions of the absorption edge and the absorption maximum in the visible region of the spectrum, respectively. For these purposes, we used a Shimadzu UV-31000 ultraviolet spectrophotometer, which made it possible to record absorption spectra in the wavelength range from 200 to 800 nm with a resolution of 1 nm.

The Raman spectra and surface enhanced Raman scattering spectra of the studied structures were recorded in the backscattering geometry under excitation by radiation from He−Cd and Ar$^+$ lasers at wavelengths of 325, 488, and 514.5 nm with LabRam and T64000 spectrometers and a triple monochromator at room temperature.

The infrared (IR) reflection/absorption spectra were measured at room temperature on a Vertex 80v vacuum Fourier transform infrared (FT−IR) spectrometer in the frequency range from 50 to 700 cm$^{-1}$. The measurements were carried out in $p$-polarized light. The angle of incidence of the light beam onto the sample was equal to 80°.

The structural parameters of the samples were determined using scanning electron microscopy (SEM) and atomic force microscopy (AFM).

## 3. RESULTS AND DISCUSSION

### 3.1. Structural Parameters

Figure 1 shows the SEM images obtained for the structure with ZnO nanorods at different angles with respect to the surface normal. It can be seen from this figure that the nanostructures consist of close-packed predominantly vertically oriented hexagonal rods with a diameter of 40−60 nm and a height of 300−500 nm.

A three-dimensional AFM image of ZnO nanocrystals is shown in Fig. 2. It can be seen from this figure that the nanocrystals have a lateral size of approximately 40 nm and an aspect ratio (i.e., the ratio of the height to the lateral size) in the range from 1/6 to 1/10. The effect of the AFM tip has raised the question as to whether the nanocrystal has the form of a truncated sphere or an ellipsoid.

The surface of structures with ZnO nanorods and nanocrystals was covered with silver nanoclusters, which, according to the SEM data, have sizes in the range from 10 to 20 nm. According to the data obtained from absorption spectroscopy in the visible spectral region, silver clusters with these sizes have the energy of localized plasmons in the range from 2.25 to 2.48 eV (from 500 to 550 nm). Correspondingly, the energy of radiation from the Ar$^+$ laser falls in this range (the excitation line at a wavelength of 514.5 nm).
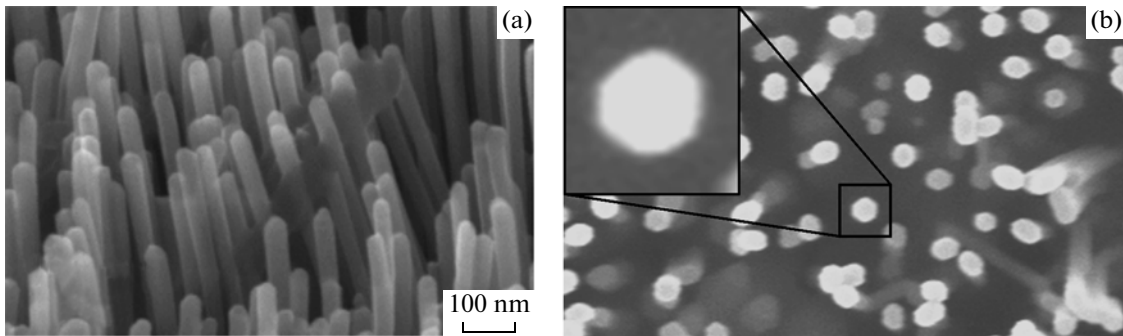
**Fig. 1.** SEM images obtained for the structure with ZnO nanorods (a) at an angle of 53° to the surface and (b) at a right angle to the surface. The inset shows the hexagonal structure of the nanorods.
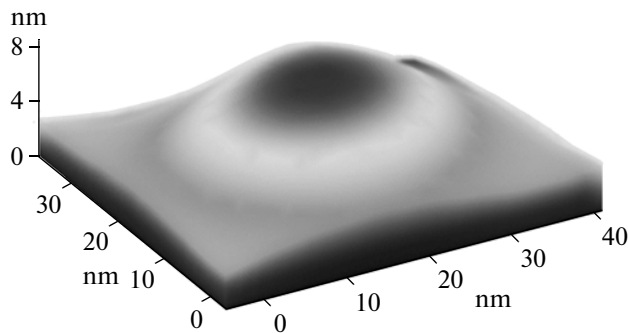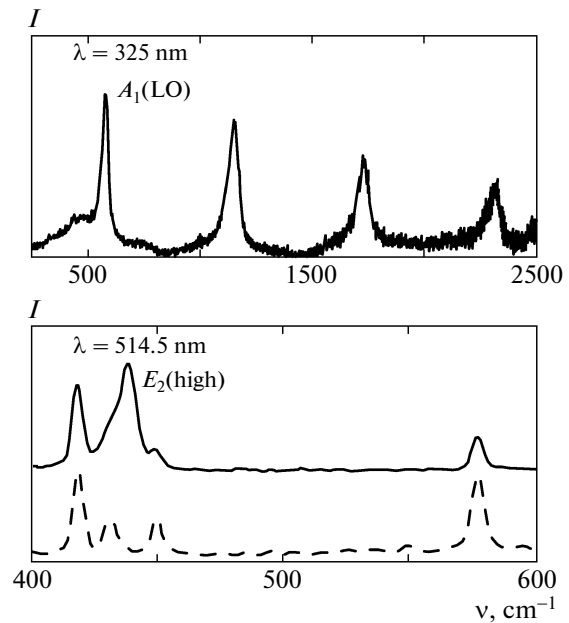


**Fig. 2.** AFM image of the ZnO nanocrystal.



**Fig. 3.** Experimental Raman spectra of the structure with ZnO nanorods measured at laser radiation wavelengths of 325 and 514.5 nm (solid lines). For comparison the dashed line shows the Raman spectrum of the sapphire substrate.

### 3.2. Raman Scattering of Light by ZnO Nanostructures

According to the selection rules for Raman scattering, the films of the ZnO compound with the hexagonal structure and the $c$ axis directed along the growth axis of the structure, in the backscattering geometry, should exhibit phonons of the symmetries $E_2$(high) and $A_1$(LO) at frequencies of 438 and 577 cm$^{-1}$, respectively [26].

Figure 3 presents the experimental Raman scattering spectra of the structures with ZnO nanorods, which were measured under the resonance (at 325 nm) and nonresonance (at 514.5 nm) conditions, in comparison with the Raman scattering spectrum of the sapphire substrate. Under the resonance conditions, i.e., when the radiation energy (3.82 eV) is close to the energy of interband electronic transitions in nanorods, the Raman scattering spectrum contains intense peaks that correspond to the optical phonon $A_1$(LO) (574 cm$^{-1}$) in ZnO [13], as well as to its overtones. The presence of a series of periodically repeating peaks of the overtones of the $A_1$(LO) phonon in the spectrum indicates a high quality of the crystal structure of the obtained nanorods. In the nonresonant Raman scattering spectra of the structures with nanorods, there is an intense peak near 438 cm$^{-1}$, which is characteristic of crystalline ZnO with hexagonal packing [10, 26] and corresponds to the $E_2$(high) phonon. Peaks at 420

and 580 cm$^{-1}$ are observed in the Raman scattering spectra of both the ZnO nanorods and the sapphire, and, consequently, they are caused by vibrations in the sapphire substrate. It should be noted that the latter peak is close to the frequency of the $A_1$(LO) phonons in ZnO and, possibly, masks the signal from nanorods.

Similar Raman spectra measured under resonance conditions have also been observed for structures with ZnO nanocrystals (Fig. 4). In this case, the exciting radiation energy (3.82 eV) is close to the energy of interband electronic transitions in nanocrystals (this energy varies in the range from 3.33 to 3.80 eV depending on the size of the nanocrystals [10]). The Raman spectrum exhibits an intense peak, which corresponds to the optical phonon $A_1$(LO), and a number of overtones of this mode, which also confirms the
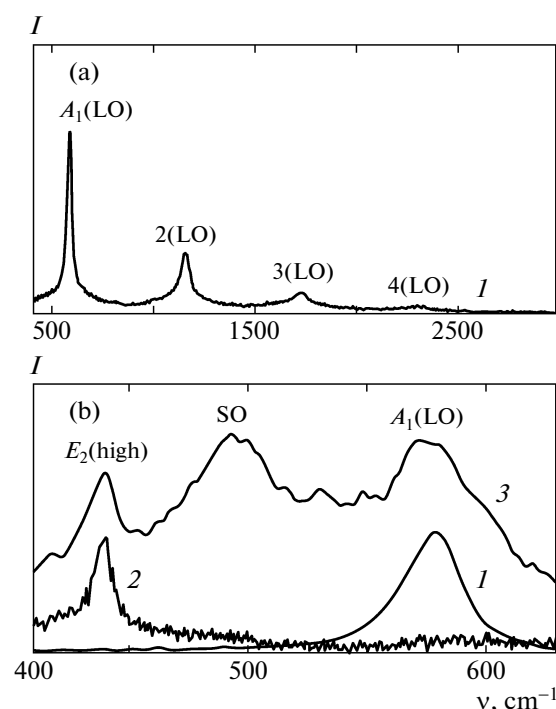
**Fig. 4.** Experimental Raman spectra of the structures with ZnO nanocrystals measured under (a) resonance and (b) nonresonance conditions and recorded at different laser radiation wavelengths $\lambda$ = (*1*) 325, (*2*) 488, and (*3*) 514.5 nm.

high quality of the crystal structure of the nanocrystals obtained in our experiments.

In the Raman spectra recorded for the sample with nanocrystals under nonresonance conditions, we have observed the modes $E_2$(high) at 438 cm$^{-1}$ (488 nm) and $A_1$(LO) near 576 cm$^{-1}$ (514.5 nm), which is characteristic of ZnO (see Fig. 4). It should be noted that the frequencies of these modes actually coincide with their bulk values [26]. This indicates that the quantum confinement effect exerts an extremely weak influence on the frequencies of optical phonons in the structures under investigation due to the in-plane dispersion of optical phonons in ZnO. A similar conclusion was drawn by Rajalakshmi et al. [18] and Lin et al. [27], who investigated ZnO nanocrystals of different sizes. It was shown that, when the size of ZnO nanocrystals decreases from 12 to 4 nm, the frequency of the $E_2$(high) mode at 438 cm$^{-1}$ decreases by only 5 cm$^{-1}$, while the frequency of the $E_1$(LO) mode decreases by 4 cm$^{-1}$ with a decrease in the nanocrystal size from 8 to 4 nm. The quantum confinement effect in the nanorods should be even less pronounced than that in the nanocrystals, because the nanorods have a substantially larger diameter. Therefore, the influence of the quantum confinement effect on the frequencies of optical phonons in ZnO nanostructures further will be ignored.

The Raman spectra recorded for the sample with nanocrystals at a wavelength of 514.5 nm additionally exhibit a broad feature (approximately 50 cm$^{-1}$) near 495 cm$^{-1}$, which is located between the frequencies of the longitudinal optical and transverse optical (TO) phonons of both the symmetry $A_1$ and the symmetry $E_1$. This mode has also been observed by other authors [28−31] and has been attributed to the surface optical (SO) phonons. In the study of ZnO submicron crystals and ZnO thin single-crystal films with submicron surface structures [18], the surface optical phonons in the Raman spectra measured at an excitation radiation wavelength of 325 nm manifested themselves in the frequency range from 457 to 468 cm$^{-1}$. According to the results obtained by Rajalakshmi et al. [18], who also investigated the influence of organic ligands on the vibrational properties of ZnO nanocrystals, in the Raman spectra (under excitation with a laser radiation at a wavelength of 647.1 nm), the surface optical phonon modes were excited near 490 cm$^{-1}$. Gupta et al. [29] measured the Raman spectra of ZnO nanorods and observed the surface optical phonon mode near 475 cm$^{-1}$. In the Raman spectra of mechanically activated ZnO nanopowders [30], the mode is excited near 510 cm$^{-1}$.

### 3.3. Surface Enhanced Raman Scattering of Light by ZnO Nanostructures and Models for the Description of Surface Modes in Nanorods and Nanocrystals

Figures 5a and 6 present the Raman spectra measured for structures with ZnO nanorods and nanocrystals, which contain silver nanoclusters deposited on their surface, in comparison with the Raman spectra of the initial structures without silver nanoclusters. In the Raman spectrum of the ZnO nanorods with silver nanoclusters (Fig. 5a), there appear new intense modes near 495 and 569 cm$^{-1}$, which were not previously observed in the Raman spectra of the initial nanorods. Here and below, the mode frequencies are obtained from the best fit of the experimental spectra by Lorentzian profiles.

Such broad lines can be explained either by the statistical spread of the size and shape of the nanorods and nanocrystals or by the presence of defects in these structures, which leads to the broadening and low-frequency shift of the lines attributed to the fundamental optical modes [32, 33]. The value of this shift depends on the dispersion of optical phonons. In the case of ZnO, optical phonons are characterized by the in-plane dispersion; consequently, the effects of disorder, as well as the effect of localization of optical phonons which was considered above, appear to be small (no more than 10 cm$^{-1}$) and do not describe the observed modes. A series of overtones of optical phonons observed at frequencies that are multiple of the frequencies of fundamental optical modes in the resonant Raman scattering spectra indicates that the nanostructures have a high crystalline quality and that
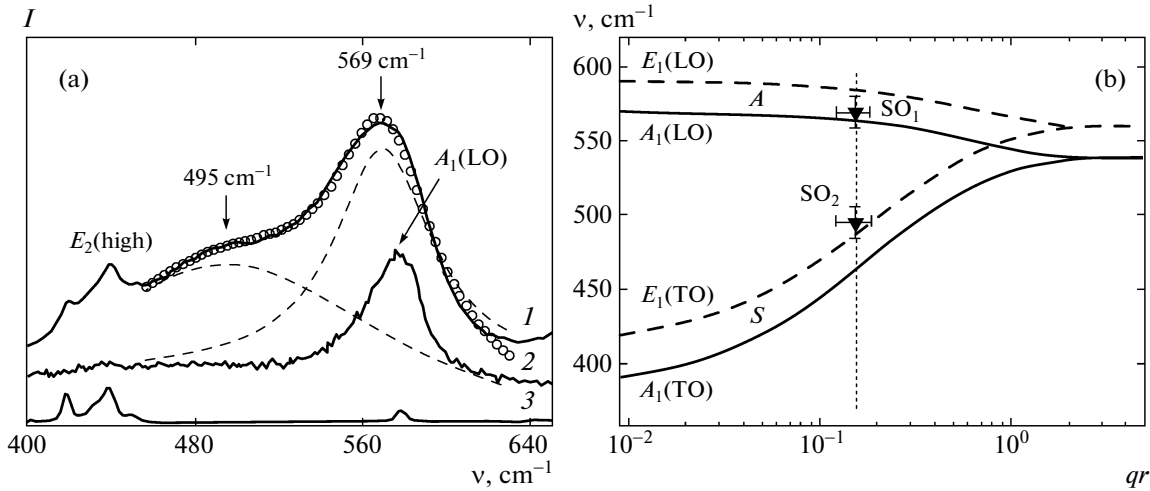
**Fig. 5.** (a) Experimental spectra of surface enhanced Raman scattering (curve *1*) and Raman scattering (curve *3*) for the structure with ZnO nanorods measured at a laser radiation wavelength of 514.5 nm. Open circles represent the results of the fitting of the surface enhanced Raman scattering spectrum by two Lorentzian profiles (dashed lines). For comparison, curve *2* shows the resonant Raman scattering spectrum of the ZnO structure without silver clusters measured at 325 nm. (b) Dispersion of the SO phonons calculated according to [35] for nanorods with a rectangular cross section. The symmetric and asymmetric dispersion branches are designated as *S* and *A*, respectively. Triangles indicate the experimental values of the frequencies of SO phonons.

the effect of disorder is very small. Furthermore, these modes are especially clearly observed in the Raman spectra of the structures in the presence of silver nanoclusters, which suggests that the observed modes have a surface character. Hence, these modes (observed near 495 and 569 cm$^{-1}$) are attributed to the surface optical phonons formed from phonons of the symmetry $A_1$ or the symmetry $E_1$. The appearance of these intense modes in the Raman spectrum of the structures in the presence of silver nanoclusters indicates the manifestation of the effect of surface enhanced Raman scattering in the structures with nanorods.

The spectra of surface optical phonon modes in nanorods have been described using the dielectric function model under the assumption that the nanorods have the form of a cylinder [34]. In this case, the material of the nanorods is assumed to be isotropic and can be described by the dielectric function in the form

$$\varepsilon(\omega) = \varepsilon_\infty \frac{\omega^2 - \omega_{LO}^2}{\omega^2 - \omega_{TO}^2}, \quad (1)$$

where $\varepsilon_\infty$ is the high-frequency dielectric function; and $\omega_{LO}$ and $\omega_{TO}$ are the frequencies of longitudinal and transverse optical phonons, respectively. The frequencies of surface optical phonons are determined by the relationship

$$\frac{\varepsilon(\omega)}{\varepsilon_m} = \frac{I_m(qr)K_m'(qr)}{I_m'(qr)K_m(qr)}, \quad (2)$$

where $I_m(qr)$ and $K_m(qr)$ are the Bessel functions ($m = 0, 1, 2, ...$), $\varepsilon_m$ is the dielectric function of the environment, $r$ is the radius of the cylinder, $q = 2\pi/\lambda$ is the wave number, and $\lambda$ is the wavelength of the laser radiation used in the experiment. According to this model,

the frequency of surface optical phonon mode at $m = 0$ takes on a single (and maximum among all modes with different $m$) value that is equal to 450 cm$^{-1}$, which is significantly lower than the frequencies of the two modes observed in the experiment. Therefore, the model of cylindrical nanorods [34] does not describe the experiment. To the best of our knowledge, no publications concerned with the calculations performed for hexagonal rods are available in the literature.

The frequencies of surface modes can be estimated within the framework of a simple model for nanorods with a rectangular cross section that provides a simple analytical solution for surface modes. Consideration of the surface optical phonon modes in nanorods with a rectangular cross section [35, 36] leads to a qualitatively new result, i.e., the splitting of the surface optical phonon mode into symmetric (low-frequency) and asymmetric (high-frequency) modes due to the lowering of the symmetry of the nanorods as compared to the symmetry of the cylindrical nanorods. A similar effect should be expected in the case of hexagonal nanorods, because their symmetry is lower than the symmetry of cylindrical nanorods. Qualitatively, this result coincides with the result obtained from calculations performed for AlN/GaN rods with the wurtzite structure [37].

Within the framework of this model, we have calculated frequencies of surface optical phonon modes in the ZnO nanorods for two sets of parameters (phonons of the symmetries $E_1$ and $A_1$). It has been assumed that the side of the rectangle, which represents a cross section of the nanorods, corresponds to the average size of the nanorods, which was determined from the SEM data. The results of the calculation of the frequencies
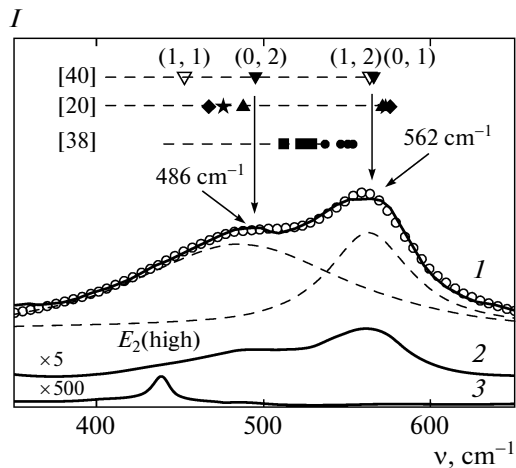
**Fig. 6.** Experimental surface enhanced Raman scattering spectra of the structure with ZnO nanocrystals measured at laser excitation wavelengths of 514.5 nm (curve *1*) and 488 nm (curve *2*). For comparison, curve *3* shows the Raman spectrum of the same ZnO structure without silver clusters. Open circles represent the results of the fitting of the surface enhanced Raman scattering spectrum (curve *1*) by two Lorentzian profiles (dashed lines). Closed squares and circles indicate the calculated (within the model proposed in [38]) frequencies of SO phonons for $l = 1, 2, 3, 4$ (the mode frequency increases with increasing number *l*) for phonons with symmetries $A_1$ and $E_1$, respectively. Closed triangles, asterisks, and rhombuses indicate the frequencies of SO phonons calculated within the model proposed in [20] for aspect ratios of 1/6, 1/8, and 1/10, respectively. The frequencies of SO phonons calculated within the model proposed in [40] for an aspect ratio of 1/10 are denoted by closed triangles ($m = 0$, $l = 1, 2$) and open triangles ($m = 1$, $l = 1, 2$), respectively.
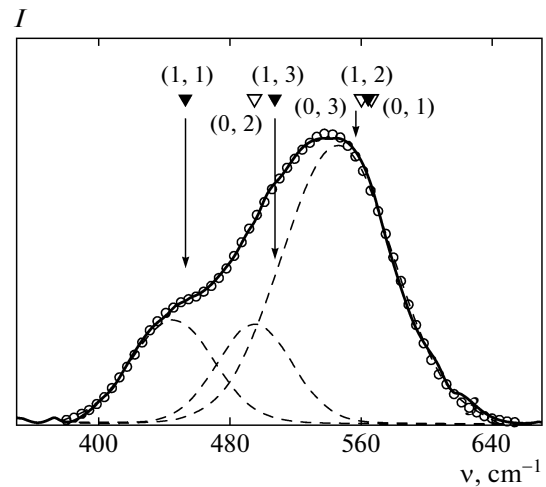


**Fig. 7.** Experimental IR absorption spectrum of the structure with ZnO nanocrystals. Open circles represent the results of the fitting of the IR absorption spectrum by three Gaussian profiles (dashed lines). Open and closed triangles indicate frequencies of modes with $m = 0$ and $l = 1$, respectively, which were determined within the model proposed in [40].

of surface optical phonon modes as a function of the size of the nanorods are presented in Fig. 5b. It can be seen from this figure that the frequencies of experimentally observed modes correspond closely to the calculated values of the symmetric and asymmetric surface optical phonon modes.

The effect of surface enhanced Raman scattering by the surface optical phonon modes is even more clearly pronounced for structures with ZnO nanocrystals (Fig. 6, curve *1*). In the surface enhanced Raman spectrum of this structure, there arise peaks at frequencies of 486 and 562 cm$^{-1}$, with the intensity at least three orders of magnitude higher than the intensity of the $E_2$(high) mode observed in the Raman spectrum of the same structure but in the absence of silver nanoclusters (Fig. 6, curve *3*). It should be noted that the observed lines are caused by precisely the inelastic scattering of light, rather than by the luminescence, because these lines manifest themselves at different wavelengths of the pump laser radiation (at 514.5 and 488 nm, as is shown in Fig. 6 by curves *1* and *2*, respectively).

Additional information on phonon modes in the structures with ZnO nanocrystals has been obtained using IR spectroscopy. In the IR absorption spectrum presented in Fig. 7, there is broad peak with an asymmetric shoulder, which is decomposed into Gaussian profiles; as a result, we have determined three modes at frequencies of 445, 495, and 550 cm$^{-1}$. The frequencies of these modes lie between the frequencies of the TO and LO phonons in ZnO. Consequently, these modes have been interpreted as the surface optical phonon modes localized in the ZnO nanocrystals. It should be noted that the modes revealed in the IR absorption spectrum at frequencies of 445 and 550 cm$^{-1}$ have not been observed in the Raman and surface enhanced Raman scattering spectra. This can be explained by different selection rules for allowed frequencies of phonons in Raman scattering and IR absorption. Since the ZnO nanorods were grown on sapphire substrates, the surface optical phonon modes of ZnO in the IR reflection spectra of these nanostructures are masked by an intense reflection from sapphire. For this reason, the IR spectra of the ZnO nanorods have not been analyzed in our present work. It should also be noted that the deposition of silver onto the surface of the nanocrystals has no noticeable influence on the IR spectra and leads only to an insignificant decrease in the signal.

For the description of the surface modes in nanocrystals, as well as in the case of the nanorods, there are a number of models. The simplest model is the model of spherical nanocrystals, which is based on the concept of nanocrystals as an isotropic dielectric continuum [38]. The dielectric function $\varepsilon(\omega)$ of the material of nanocrystals is described by expression (1). The fre-

quencies of the LO and TO phonons are related by the Lyddane−Sachs−Teller relation

$$\frac{\omega_{LO}^2}{\omega_{TO}^2} = \frac{\varepsilon_0}{\varepsilon_\infty}, \qquad (3)$$

where $\varepsilon_0$ is the static dielectric constant.

Taking into account the electrostatic boundary conditions, we have determined the condition providing for the existence of surface phonons in spherical quantum dots:

$$\varepsilon(\omega) = -\frac{l+1}{l}\varepsilon_m, \quad l = 1, 2, 3, \ldots, \qquad (4)$$

where $l$ is the quantum number.

By equating expressions (1) and (4) and taking into account expression (3), we can write the frequencies of surface optical phonons in the form

$$\omega_{SO} = \omega_{TO}\sqrt{\frac{l\varepsilon_0 + (l+1)\varepsilon_m}{l\varepsilon_\infty + (l+1)\varepsilon_m}}. \qquad (5)$$

This expression has been used to calculate the frequencies of the surface optical phonons in spherical ZnO nanocrystals, which originate from optical phonons of the symmetries $A_1$ and $E_1$, with the parameters taken from [39]. The results obtained from calculations for the first four modes of surface optical phonons with the use of two sets of parameters are presented in Fig. 6. With an increase in the mode number, the frequency of surface optical phonons formed from phonons of both the symmetry $A_1$ and the symmetry $E_1$ increases. As can be seen from this figure, the calculated frequencies of surface optical phonons differ from the experimental data. A possible reason for this discrepancy can be provided by the deviation of the shape of real nanocrystals from the spherical shape, as well as by the fact that the dielectric function of the material of nanocrystals is considered to be isotropic. Consequently, we have used the models proposed in [20, 40], which are applicable to anisotropic nanocrystals in the form of a disk and an ellipsoid.

In the model described by Chassaing et al. [20], the inclusion of anisotropy in the calculation performed for a flat disk leads to two solutions of the equation relating the frequency of surface optical phonons and the aspect ratio (of the height of the disk to its diameter). The frequencies of the optical phonons have been calculated within the framework of this model for aspect ratios of 1/6, 1/8, and 1/10, which are close to the corresponding values obtained from the AFM data for the ZnO nanocrystals under investigation. The frequencies of the calculated modes for these three values of the aspect ratio are presented above in Fig. 6. It can be seen from this figure that the frequencies of the surface optical phonon modes with an aspect ratio of 1/6 are in the best agreement with the Raman data. However, the model under consideration disregards the effect of confinement of optical and surface phonons and, consequently, does not describe the surface opti-

cal phonon modes, which are additionally observed in the IR spectrum.

It is known [40−43] that the spectrum of surface phonons in ellipsoidal nanocrystals represents a set of modes described by two quantum numbers, i.e., $m = 0$, 1, 2, ... and $l = 1, 2, 3, \ldots$. The model proposed by Fonoberov and Balandin [40] allows one to determine the frequencies of these modes in anisotropic ZnO nanocrystals. The components of the permittivity tensor for this case can be written in the form

$$\varepsilon_\perp(\omega) = \varepsilon_\perp(\infty)\frac{\omega^2 - \omega_{\perp, LO}^2}{\omega^2 - \omega_{\perp, TO}^2}, \qquad (6)$$

$$\varepsilon_z(\omega) = \varepsilon_z(\infty)\frac{\omega^2 - \omega_{z, LO}^2}{\omega^2 - \omega_{z, TO}^2}, \qquad (7)$$

where $z$ is the direction along the minor semiaxis of the oblate ellipsoid; and $\omega_{\perp, LO(TO)}$ and $\omega_{z, LO(TO)}$ are the frequencies of the LO(TO) phonons of the symmetries $E_1$ and $A_1$, respectively.

Using the Maxwell's equations and boundary conditions, we have obtained an expression that, in the implicit form, relates the frequency of surface phonons and the ratio of the major semiaxes of the ellipsoid for particular quantum numbers $l$ and $m$ (coefficients of the associated Legendre functions). Following the work by Fonoberov and Balandin [40], we have determined the frequencies of surface optical phonons with quantum numbers $m = 0$, 1 and $l = 1, 2$ in ellipsoidal ZnO nanocrystals for different aspect ratios (1/6−1/10). The best agreement between the calculated and experimental data is observed for the aspect ratio of 1/10. The frequencies of surface optical phonon modes thus obtained are presented in Figs. 6 and 7 and denoted as $(m, l)$.

In the experiments on Raman scattering and IR absorption in nanoclusters, one can observe surface modes that have different symmetries (and, correspondingly, different values of $l$ and $m$). In particular, according to the work by Comas et al. [43], the surface optical phonon modes with $l = 0$ and even numbers $m$ should be observed in the experiments on Raman scattering of light by ellipsoidal nanocrystals. However, in our case, the shape of ZnO nanocrystals differs from ellipsoidal and the selection rules for Raman scattering weaken. Therefore, in the IR absorption and Raman scattering spectra, there will appear, first of all, the modes with small quantum numbers (i.e., $m = 0$, 1 and $l = 1, 2$). It can be seen from Fig. 6 that the modes $(0, 1)$ and $(1, 2)$ can be responsible for the observation of the peak at 562 cm$^{-1}$, whereas the peak at 486 cm$^{-1}$ corresponds to the $(0, 2)$ mode. At the same time, the $(1, 1)$ mode does not manifest itself in the Raman spectrum.

The modes with a dipole moment should first of all be observed in the IR spectra. Among these modes are those with odd quantum numbers. As can be seen from Fig. 7, the peak at 550 cm$^{-1}$ can be attributed to three

modes, i.e., (0, 1), (1, 2), and (0, 3). The "shoulder" at 495 cm$^{-1}$, most likely, can be due to the absorption of light by the (1, 3) mode, because the (0, 2) mode, even though has almost the same frequency, is totally symmetric and, therefore, should not manifest itself in the IR spectra. The feature observed in the IR spectrum at 445 cm$^{-1}$, apparently, corresponds to the (1, 1) mode.

Therefore, the model of ellipsoidal nanocrystals [40] consistently describes both the IR spectra and the experiments on Raman scattering of light by ZnO nanocrystals.

## 4. CONCLUSIONS

Thus, we have investigated the resonant and non-resonant Raman light scattering by optical phonons, the surface enhanced Raman scattering by surface phonons of ZnO nanorods and nanocrystals, and the IR absorption by surface phonons in ZnO nanocrystals. It has been established that the deposition of silver clusters onto the surface of nanostructures leads either to an abrupt increase (by a factor of 10$^3$) in the intensity of lines attributed to the surface phonons observed in the Raman spectra or to the appearance of new modes of surface phonons. It has been demonstrated that the effective dielectric function model can be successfully applied to the description of the spectra of surface phonons in ZnO nanorods and nanocrystals. The calculation of the surface mode frequencies, which was carried out under the assumption that the nanorods have a rectangular cross section, describes fairly well the frequencies of experimental modes observed in the surface enhanced Raman scattering spectra of the ZnO nanorods. The frequencies of the surface modes observed in both the surface enhanced Raman scattering spectra and the IR absorption spectra of ZnO nanocrystals are adequately described within the framework of the model of anisotropic ellipsoidal ZnO nanocrystals considered in [40].

## REFERENCES

1. I. R. Nabiev, R. G. Efremov, and G. D. Chumanov, Sov. Phys.—Usp. **31** (1), 1 (1988).

2. J. Kneipp, B. Wittig, H. Bohr, and K. Kneipp, Theor. Chem. Acc. **125**, 319 (2010).

3. M. Moskovits, Rev. Mod. Phys. **57**, 783 (1985).

4. W.-H. Park and Z. H. Kim, Nano Lett. **10**, 4040 (2010).

5. K. Kneipp, Y. Wang, H. Kneipp, L. T. Perelman, I. Itzkan, R. R. Dasari, and M. S. Feld, Phys. Rev. Lett. **78**, 1667 (1997).

6. M. Moskovits, in *Surface-Enhanced Raman Scattering: Physics and Applications*, Ed. by K. Kneipp, M. Moskovits, and H. Kneipp (Springer, Berlin, 2006), p. 1.

7. A. G. Milekhin, R. J. Meijers, T. Richter, R. Calarco, S. Montanari, H. Lüth, B. A. P. Sierra, and D. R. T. Zahn, J. Phys.: Condens. Matter **18**, 5825 (2006).

8. A. G. Milekhin, L. L. Sveshnikova, T. A. Duda, N. V. Surovtsev, S. V. Adichtchev, and D. R. T. Zahn, JETP Lett. **88** (12), 799 (2008).

9. S. Lefrant, J. P. Buisson, J. Schreiber, J. Wery, E. Faulques, O. Chauvet, M. Baibarac, and I. Baltog, in *Spectroscopy of Emerging Materials*, Ed. by E. C. Faulques, D. L. Perry, and A. V. Yeremenko, in *NATO Science Series II: Mathematics, Physics, and Chemistry* (Kluwer, Dordrecht, 2004), p. 127.

10. C. F. Klingshirn, B. K. Meyer, A. Waag, A. Hoffman, and J. M. M. Geurts, *ZnO: From Fundamental Properties towards Novel Applications* (Springer, Berlin, 2010).

11. B. Cheng, Y. Xiao, G. Wu, and L. Zhang, Appl. Phys. Lett. **84**, 416 (2004).

12. X. Wang, Q. Li, Z. Liu, J. Zhang, Z. Liu, and R. Wang, Appl. Phys. Lett. **84**, 4941 (2004).

13. H. J. Fan, B. Fuhrmann, R. Scholz, C. Himcinschi, A. Berger, H. Leipner, A. Dadgar, A. Krost, S. Christiansen, U. Gösele, and M. Zacharias, Nanotechnology **17**, S231 (2006).

14. V. A. Fonoberov and A. A. Balandin, Appl. Phys. Lett. **85**, 5971 (2004).

15. K. A. Alim, V. A. Fonoberov, and A. A. Balandin, Appl. Phys. Lett. **86**, 053103 (2005).

16. B. Kumar, H. Gong, S. Y. Chow, S. Tripathy, and Y. Hua, Appl. Phys. Lett. **89**, 071922 (2006).

17. H.-M. Cheng, K.-F. Lin, H.-C. Hsu, and W.-F. Hsieh, Appl. Phys. Lett. **88**, 261909 (2006).

18. M. Rajalakshmi, A. K. Arora, B. S. Bendre, and S. Mahamuni, J. Appl. Phys. **87** (5), 2445 (2000).

19. P.-M. Chassaing, F. Demangeot, V. Paillard, A. Zwick, N. Combe, C. Pagès, M. L. Kahn, A. Maisonnat, and B. Chaudret, Appl. Phys. Lett. **91** (5), 053108 (2007).

20. P.-M. Chassaing, F. Demangeot, V. Paillard, A. Zwick, N. Combe, C. Pagès, M. L. Kahn, A. Maisonnat, and B. Chaudret, Phys. Rev. B: Condens. Matter **77** (15), 153306 (2008).

21. C. Y. Liu, M. M. Dvoynenko, M. Y. Lai, T. H. Chan, Y. R. Lee, J.-K. Wang, and Y. L. Wang, Appl. Phys. Lett. **96**, 033109 (2010).

22. S. K. Panda and C. Jacob, Appl. Phys. A: Mater. Sci. Process. **96**, 805 (2009).

23. X. Wang, X. Kong, Y. Yu, and H. Zhang, J. Phys. Chem. C **111**, 3836 (2007).

24. G. Shan, L. Xu, G. Wang, and Y. Liu, J. Phys. Chem. C **111**, 3290 (2007).

25. C. C. Wu, D. S. Wuu, P. R. Lin, T. N. Chen, and R. H. Horng, J. Nanosci. Nanotechnol. **10** (6), 3001 (2010); C. C. Wu, D. S. Wuu, P. R. Lin, T. N. Chen, and R. H. Horng, Cryst. Growth Des. **9**, 4555 (2009).

26. H. Harima, J. Frandon, F. Demangeot, and M. A. Renucci, in *III-Nitride Semiconductors: Optical Properties I*, Ed. by M. O. Manasreh (Taylor and Francis, New York, 2002), p. 283.

27. K.-F. Lin, H.-M. Cheng, H.-C. Hsu, and W.-F. Hsieh, Appl. Phys. Lett. **88** (26), 263117 (2006).

28. H. F. Liu, S. Tripathy, G. X. Hu, and H. Gong, J. Appl. Phys. **105**, 053507 (2009).

29. V. Gupta, P. Bhattacharya, Yu. I. Yuzuk, K. Sreenivas, and R. S. Katiyar, J. Crystal Growth **287** (1), 39 (2006).

30. M. Šćepanović, M. Grujić-Brojčin, K. Vojisavljević, S. Bernik, and T. Srećković, J. Raman Spectrosc. **41** (9), 914 (2010).

31. R. Ruppin and R. Englman, Rep. Prog. Phys. **33**, 149 (1970).

32. L. A. Falkovsky, Phys.—Usp. **47** (3), 249 (2004).

33. L. A. Falkovsky, JETP **102** (1), 155 (2006).

34. V. E. Sernelius, *Surface Modes in Physics* (Wiley, Berlin, 2001).

35. M. A. Stroscio, K. W. Kim, M. A. Littlejohn, and H. Chuang, Phys. Rev. B: Condens. Matter **42**, 1488 (1990).

36. Q. Xiong, J. Wang, O. Reese, L. C. Lew Yan Voon, and P. C. Eklund, Nano Lett. **4**, 1991 (2004).

37. L. Zhang, J.-J. Shi, and T. L. Tansley, Phys. Rev. B: Condens. Matter **71**, 245324 (2005).

38. E. Menéndez, C. Trallero-Giner, and M. Cardona, Phys. Status Solidi B **199** (1), 81 (1997).

39. E. F. Venger, A. V. Melnichuk, L. Y. Melnichuk, and Yu. A. Pasechnik, Phys. Status Solidi B **188**, 823 (1995).

40. V. A. Fonoberov and A. A. Balandin, J. Phys.: Condens. Matter **17**, 1085 (2005).

41. P. A. Knipp and T. L. Reinecke, Phys. Rev. B: Condens. Matter **46**, 10310 (1992).

42. M. Yu. Ladanov, A. G. Milekhin, A. I. Toropov, A. K. Bakarov, A. K. Gutakovskii, D. A. Tenne, S. Schulze, and D. R. T. Zahn, JETP **101** (3), 554 (2005).

43. F. Comas, C. Trallero-Giner, N. Studart, and G. E. Marques, Phys. Rev. B: Condens. Matter **65**, 073303 (2002).

*Translated by O. Borovik-Romanova*